Available online at www.sciencedirect.com
ScienceDirect
Journal of Magnetic Resonance 192 (2008) 112–122
JMR Journal of Magnetic Resonance
www.elsevier.com/locate/jmr

# Comparison of several hetero-nuclear dipolar recoupling NMR methods to be used in MAS HMQC/HSQC

B. Hu, J. Trébosc, J.P. Amoureux *

*UCCS, CNRS-8181, Lille University, Fr-59652 Villeneuve d'Ascq Cedex, France*

Received 22 November 2007; revised 5 February 2008
Available online 12 February 2008

**Abstract**

We compare several hetero-nuclear dipolar recoupling sequences available for HMQC or HSQC experiments applied to spin-1/2 and quadrupolar nuclei. These sequences, which are applied to a single channel, are based either on the rotary resonance recoupling ($R^3$) irradiation, or on two continuous rotor-synchronized modulations ($SFAM_1$ and $SFAM_2$), or on four symmetry-based sequences ($R2_1^1, SR4_1^2, R12_3^5, R20_5^9$), or on the REDOR scheme. We analyze systems exhibiting purely hetero-nuclear dipolar interactions as well as systems where homo-nuclear dipolar interactions need to be canceled. A special attention is given to the behavior of these sequences at very fast MAS. It is shown that $R^3$ methods behave poorly due to the narrowness of their rf-matching curves, and that the best methods are $SR4_1^2$ and SFAM ($SFAM_1$ or $SFAM_2$ if homo-nuclear interactions are not negligible). REDOR can also recouple efficiently hetero-nuclear dipolar interactions, provided the sequence is sent on the non-observed channel and homo-nuclear dipolar interactions are negligible. We anticipate that at ultra-fast spinning speed, $SFAM_1$ and $SFAM_2$ will be the most efficient methods.


*Keywords:* HMQC; HSQC; Quadrupolar nuclei; Heteronuclei dipolar recoupling methods

## 1. Introduction

In liquid-state, hetero-nuclear multiple- (*J*-HMQC) [1] or single- (*J*-HSQC) [2] quantum coherence through-bond *J*-coupling methods, which will be denoted *J*-H-M/S-QC when considered together, have been designed to enhance the signal by inverse detection.

In solids, nuclei are submitted to several anisotropic interactions, which lead to broad resonances and thus very poor signal to noise ratios. To enhance the resolution and increase the signal to noise ratio, sample-rotation at the magic-angle (MAS: magic-angle spinning) [3] is used. To further enhance the low sensitivity of NMR in solids, cross-polarization (CP) is also often used [4]. Nuclear polarization is then usually transferred through the dipolar interaction from 'strong' abundant spins I to 'weak' diluted spins S, to increase the magnetization of S and the repetition rate of the experiment. Nowadays, CP is often combined with MAS for resolution enhancement, leading to CP-MAS experiments [5]. Another way to enhance the sensitivity is to combine the indirect detection methods with MAS, leading to MAS *J*-HMQC [6] and MAS *J*-HSQC [7] experiments, to obtain through-bond hetero-nuclear correlation (MAS *J*-HETCOR) 2D spectra under high-resolution. Recently, it has been shown that with a very slight change of the pulse sequences these methods can be adapted to observe through-space MAS *D*-HETCOR 2D spectra, leading to MAS *D*-H-M/S-QC experiments [8]. Usually, dipolar interactions are cancelled by the MAS rotation. Several different methods exist for hetero-nuclear recoupling purposes. This re-introduction has been performed first with the rotary-resonance recoupling ($R^3$) method [9], and then several symmetry-based sequences have been proposed: e.g $R12_3^1, R12_3^5$, and $R20_5^9$ [10,11]. Another symmetry-based sequence, $SR4_1^2$, has been recently introduced in the context of measuring the OH distances in samples with numerous protons, but its application to

* Corresponding author. Fax: +33 3 20 43 68 14.
*E-mail address:* jean-paul.amoureux@univ-lille1.fr (J.P. Amoureux).

1090-7807/$ - see front matter © 2008 Elsevier Inc. All rights reserved.
doi:10.1016/j.jmr.2008.02.004

hetero-nuclear recoupling is quite general [12]. Very recently, Cavadini et al. published the application of the $R20_5^9$ sequence to the $^{14}$N-$^{1}$H dipolar recoupling [13]. In this article we would like to compare the advantages and limitations of these dipolar recoupling methods in the context of MAS *D*-H-M/S-QC experiments: the $R^3$ continuous irradiation, the previous three symmetry-based sequences ($SR4_1^2, R12_3^5, R20_5^9$) as well as $R2_1^1$ sequence [10,14], the standard REDOR (Rotational Echo Double Resonance) [15] and the SFAM (Simultaneous Frequency and Amplitude Modulation) concept [16], which has been proposed to overcome REDOR limitations at very fast MAS. The comparison of these hetero-nuclear dipolar recoupling methods will be made in the case of nuclei also submitted or not to large homo-nuclear dipolar-interactions. A special attention will be given to the behavior of these sequences at ultra fast MAS ($\nu_R > 40$ kHz).

## 2. Dipolar recoupling pulse sequences

Our purpose is to apply these *D*-H-M/S-QC methods in between spin-1/2 and quadrupolar nuclei. The spin value of the quadrupolar nuclei is larger than 1/2, and these systems thus present more than two Zeeman energy levels. Manipulation of the quadrupolar nucleus density matrix is thus difficult and in order to increase the efficiency of the methods, the number of pulses sent on quadrupolar nuclei must be minimized. Therefore, in the following, the dipolar recoupling sequences will always be applied to a single channel, which will be that of the spin-1/2 nucleus in case of *D*-HETCOR experiments involving quadrupolar nuclei.

Most hetero-nuclear dipolar recoupling sequences with rf field applied to a single channel automatically reintroduce the chemical shift anisotropy (CSA) on this channel because of identical rotation properties under the rf and MAS of these two interactions. In *D*-H-M/S-QC experiments, the CSA of the S observed nucleus ($CSA_S$) is refocused, but only at the very end of the sequence. To avoid any effect of $CSA_S$, its evolution must thus be perfectly identical during the two recoupling periods. One can thus anticipate that the defaults of each particular recoupling sequence will be emphasized by the re-introduction of $CSA_S$, when this sequence is performed on the observed channel, particularly in case of strong $CSA_S$. In Fig. 1 we have represented the pulse-sequences corresponding to MAS *D*-HMQC (Fig. 1a and b) and MAS *D*-HSQC (Fig. 1c and d) in case of a spin-1/2 and a half-integer quadrupolar nucleus. In case of two spin-1/2 nuclei, the recoupling sequences can be sent on any channel. It must be noted that to add constructively the dipolar dephasings related to the two recoupling sequences (for non γ-encoded sequences, see Section 2.4), the delay between these sequences must be rotor-synchronized ($kT_R$), and the π pulse (HMQC) on the S channel must be in the middle of this delay. Of course, the $t_1$ time should be also rotor-synchronized if spinning sidebands are to be avoided (e.g. for $^{14}$N indirect detection) [13,17].

### 2.1. REDOR

The rotational echo double resonance (REDOR) sequence applies evenly spaced π-pulses (two per rotor cycle) for dipolar recoupling. The π-pulses alternate the sign of hetero-nuclear dipolar dephasings modulated under MAS, hence preventing their complete averaging. REDOR is a very simple and efficient method when only hetero-nuclear interactions are taken into account. Unfortunately, when REDOR pulses are applied to the observed channel, the remaining value of $CSA_S$ at the beginning of acquisition depends critically on the rotor position with respect to the multiple π-pulse sequence. Small MAS frequency drifts and fluctuations accumulate timing errors over the long transfer periods and consequently result in incomplete and unstable $CSA_S$ refocusing. The phases of these π pulses can be calculated to compensate partly for the flip angle error, the off-resonance effect, and the fluctuation of rf-field, leading to sequences $REDOR_{XYk}$ ($k = 4, 8, 16$) [18]. However, it has been shown in case of weak dipolar recoupling, that even with these compensated sequences, a very tiny 0.1 Hz change of MAS frequency can attenuate signal intensities if all REDOR pulses are sent on the observed channel [19]. In any case, it has been shown that the hetero-nuclear dipolar recoupling decreases at very fast spinning speed when the fraction of the rotor period occupied by the two π pulses increases, especially in homo-nuclear systems [20]. REDOR presents the advantage of a longitudinal two-spin-order ($I_zS_z$) recoupling of the hetero-nuclear dipolar interactions between I and S spins in first order, which means that this interaction commutes for different spin pairs. Non-commuting dipolar interactions on the other hand lead to 'dipolar truncation', i.e. the measurement of a weak dipolar coupling between two spins is prevented if one or both spins are also strongly dipolar coupled to other spins [21]. When REDOR pulses are applied to the non-observed I channel, REDOR recouples simultaneously the $CSA_I$, but this commutes with the hetero-nuclear dipolar interaction, and thus, in practice the hetero-nuclear recoupling is not influenced by $CSA_I$. REDOR also recouples the I-spin homo-nuclear dipolar couplings, and the size of the recoupled terms depends on the ratio of the duration of the π pulses with respect to the period of the sample rotation. Hence, only in the limit of short pulses with respect to the rotation period, homo-nuclear I-spin decoupling is achieved, while under very fast MAS substantial recoupling of the I-spin homo-nuclear dipolar interactions occurs [22]. It must be noted that $REDOR_{XYk}$ ($k = 4, 8, 16$) sequences can also be viewed as $RN_n^v$ sequences (see Section 2.4) [10].

### 2.2. Rotary resonance recoupling ($R^3$)

Rotary resonance recoupling ($R^3$) has been shown to recover various anisotropic spin interactions under MAS with resonance conditions described by a number $q = \nu_1/\nu_R$ (where $\nu_1$ is the rf-strength) [9]. For CSA and hetero-

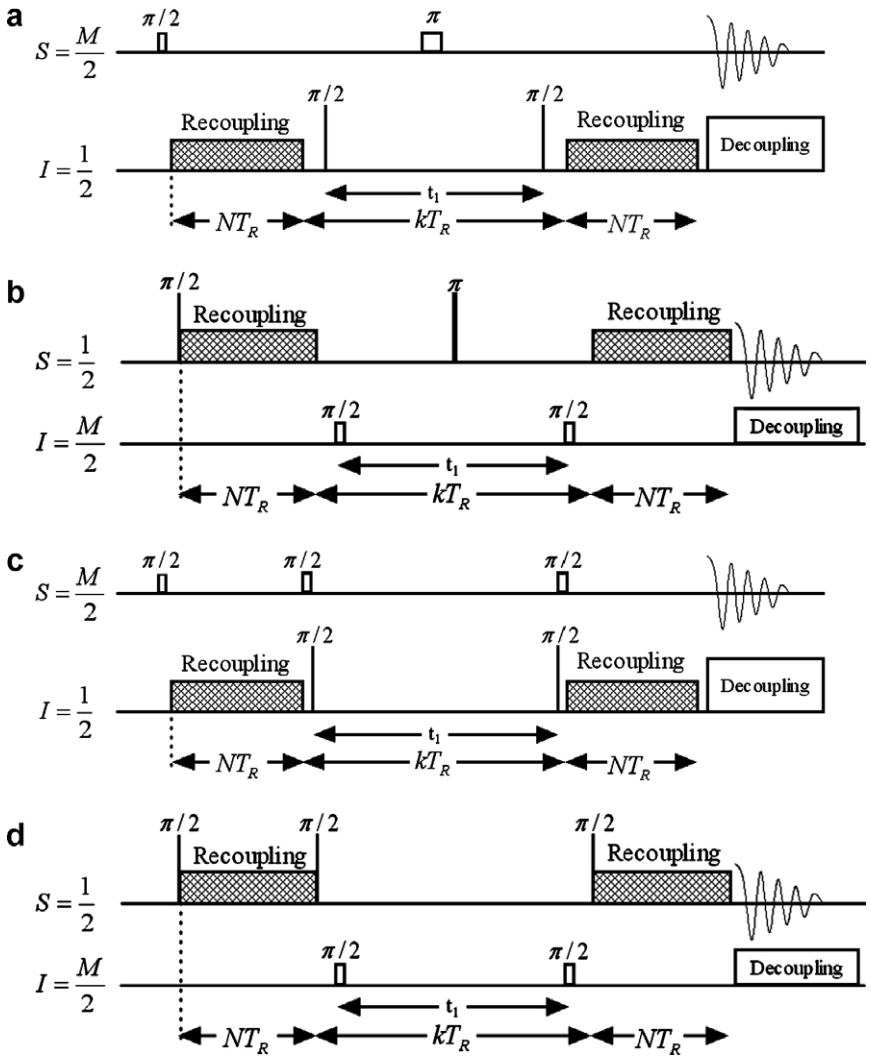


Fig. 1. HMQC pulse-sequence with recoupling on I (a) (non-observed) or S (b) (observed) spin-1/2 nuclei. HSQC pulse-sequence with recoupling on I (c) or S (d) spin-1/2 nuclei. Pulses with large rectangle are CT (central transition) selective pulses used for spins M/2. Phases of π and π/2 pulses follow the regular *J*-HMQC ones. The phase for $R^3$ is zero and the phases for other recoupling sequences are calculated according to their corresponding definitions.

nuclear dipolar coupling, the re-introduction occurs without 'dipolar truncation' at $q = 1$ and 2. For homo-nuclear dipolar coupling it occurs at $q = 1/2$ and 1 due to the bilinear nature of the spin operator in the dipolar Hamiltonian. The $q = 1/2$ resonance affects only the homo-nuclear dipolar interaction and is known as the HORROR condition [23]. It is well-known that the $q = 2$ condition reintroduces the hetero-nuclear dipolar coupling under MAS, but not the homo-nuclear interaction [17]. This condition should thus be used in case of nuclei submitted to strong homo-nuclear dipolar interaction. In other cases, the $q = 1$ condition should be preferred, because of its better experimental efficiency. $R^3$ can also be seen as symmetry based sequences $R2_1^0(q = 1)$ or $R4_1^0(q = 2)$ (see Section 2.4).

### 2.3. SFAM

At very fast spinning speeds (up to $\nu_R \approx 100$ kHz, presently), which are necessary to suppress CSA in high static magnetic fields (up to $B_o = 23.5$ T), REDOR suffers from artifacts because of the finite π pulse lengths, which represent a non negligible fraction of the rotational period. To overcome this limitation a method with 'simultaneous frequency and amplitude modulation' (SFAM) has been proposed [16]. The carrier frequency ($\nu_0 + \Delta\nu_0(t)$) of the rf field is modulated cosinusoidally, while its amplitude ($\nu_1(t)$) is modulated sinusoidally. It has been shown that the best efficiency for the hetero-nuclear dipolar recoupling is observed when the modulation frequency of this rf field is equal to the spinning speed leading to the $SFAM_1$ method:

$$\Delta\nu_0(t) = \Delta\nu_0^{\max}\cos(2\pi\nu_R t)$$
$$\nu_1(t) = \nu_1^{\max}\sin(2\pi\nu_R t) \quad (1)$$

It has also been shown that, with respect to hetero-nuclear dipolar interaction, continuous $SFAM_1$ behaves exactly the same as REDOR with ideal π pulses [16]. However, $SFAM_1$ also recouples the homo-nuclear dipolar interactions, and thus should not be used when these are

not negligible. In this case, in a similar way as with $R^3$ to eliminate homo-nuclear dipolar interactions, the modulation frequency should be twice the spinning speed, leading to the $SFAM_2$ method:

$$\Delta\nu_0(t) = \Delta\nu_0^{\max}\cos(4\pi\nu_R t)$$
$$\nu_1(t) = \nu_1^{\max}\sin(4\pi\nu_R t) \quad (2)$$

In both cases, the best efficiency is observed when the depth of the frequency modulation ($\Delta\nu_0^{\max}$) and the maximum amplitude of the rf field ($\nu_1^{\max}$) are of sufficient amplitude. It has been shown that SFAM methods do not suffer from 'dipolar truncation' [16].

### 2.4. Symmetry-based sequences

The nuclear spin interactions may be classified in terms of their properties under rotations by the quantum numbers $\{l, m, \lambda, \mu\}$, where $\{l, m\}$ and $\{\lambda, \mu\}$ denote the rank and component with respect to sample spatial rotation and spin-rotation, respectively. Selection rules have been established, which predict if a certain interaction with the quantum numbers $\{l, m, \lambda, \mu\}$ is present (symmetry-allowed) in the first-order average Hamiltonian derived under a sequence $RN_n^\nu$ ($N$ even) or $CN_n^\nu$ with the set of numbers: $N$, $n$, $\nu$ [10,14]. The basic bloc of these sequences extends over $n$ rotor periods and is composed of $N$ rotor-synchronized $\pi$ ($2\pi$ for $CN_n^\nu$) rotation elements: single-, composite-, or smoothly-modulated rf-pulses. The sequences are called '$\gamma$-encoded' when only the *phase* of the average Hamiltonian depends on the Euler angle $\gamma_{MR}$, which is one of the three angles defining the molecular orientation with respect to the rotor-frame. '$\gamma$-encoding' generally leads to a low sensitivity to synchronization of delays, high efficiency in a powder and good discrimination of the recoupled interactions [24]. On the other-hand, non-$\gamma$-encoded sequences are generally more robust as regard to rf missettings and inhomogeneity, and superior for long-range distance estimations [25]. In their simplest forms,$RN_n^\nu$ sequences are composed of $\pi$ pulses with alternate phases $\pm\pi\nu/N$. In this case, when $N = 2\nu$, the pulse phases are $\pm 90°$ and hence the phase shift in between two consecutive pulses is equal to 180°. The $RN_n^{N/2}$ sequences are then called 'amplitude modulated' and are compensated for rf-inhomogeneity [26]. Another advantage of these sequences is that $\pm 90°$ phases are easy to obtain accurately and with a fast commutation time in between them, even on old consoles. But they are not '$\gamma$-encoded'.

In this article, we are interested by hetero-nuclear dipolar recoupling $RN_n^\nu$ sequences.

This recoupling can be accomplished either with single-quantum coherences or with longitudinal two-spin-order. This leads to dipolar 'truncated' or 'not truncated' sequences, respectively. When the recoupling sequence is sent on the non-observed channel, $CSA_I$ and hetero-nuclear dipolar interactions are always recoupled simultaneously, because they have the same ranks $l = 2$, $\lambda = 1$. If these two interactions commute, hetero-nuclear dipolar recouplings are then insensitive to $CSA_I$.

We have chosen to only use $RN_n^\nu$ sequences which have been designed: (i) to use only $\pi$ pulses, (ii) to prevent 'dipolar truncation', to provide: (iii) hetero-nuclear, but (iv) not homo-nuclear dipolar recoupling, and (v) to be uncorrelated to the irradiated-spin CSA. As we wish these sequences working at very fast MAS, we have added a last criterion: to only select $RN_n^\nu$ sequences requiring a limited rf-field amplitude: $\nu_1/\nu_R = N/2n \leqslant 2$.

We have chosen to investigate the $R12_3^5$ and $R20_5^9$ sequences that have been proposed for this purpose [10,13,14]. These sequences correspond to $\pi$ pulses with $\pm 75°$ and $\pm 81°$ phases, for $R12_3^5$ and $R20_5^9$, respectively. However, the duration of the whole $RN_n^\nu$ bloc is given by $nT_R$, and it may be useful to use a shorter one in case of large hetero-nuclear dipolar interactions and/or slow spinning speed. The eight $\pi$-pulse $(\pi_x\pi_{-x}\pi_x\pi_{-x}\pi_{-x}\pi_x\pi_{-x}\pi_x)SR4_1^2$ sequence, only lasts two rotor-periods. It has been recently proposed to measure $^{17}O$–$^1H$ distances in protonated samples, but with a better discrimination of simultaneous long and short O–H distances than $R12_3^5$ [12]. Another advantage of $SR4_1^2$ is that it is an 'amplitude-modulated' sequence which means compensated for rf-inhomogeneity, as $R12_3^5$ and $R20_5^9$ sequences [10]. In the Levitt symmetry-based analytical calculations, these three non '$\gamma$-encoded' recoupling sequences ($SR4_1^2, R12_3^5$ and $R20_5^9$) require the rf-field strength to be only twice the spinning frequency: $\nu_1 = 2\nu_R$. It can be noticed that the plain $R4_1^2$ sequence can be considered as a simplified version of $SFAM_2$. Indeed, $R4_1^2$ is composed of four pulses with alternating phases ($\pm 90°$) per rotor period, which can be developed as a Fourier-series expansion ($\pm 2\nu_R$, $\pm 6\nu_R$, $\pm 10\nu_R$,...), with the first term ($\pm 2\nu_R$) being the largest. For each crystallite, the resonance frequency is always sweeping in a rotor-synchronized way due to the MAS rotation and anisotropic interactions. However, $SFAM_2$ also introduces an additional frequency sweep of the irradiation through the resonance frequency. This analogy is similar to that in between FAM [27] and DFS [28] for signal enhancement of quadrupolar nuclei. In the same way, the analogous of $SFAM_1$ is the $R2_1^1$ sequence, which also recouples the homo- and hetero-nuclear dipolar interactions and is composed of two $\pi$ pulses of opposite phases per rotor period with $\nu_1 = \nu_R$ with the Levitt's calculations [10,14].

## 3. Simulations

### 3.1. Hetero-nuclear recoupling

We have chosen to calculate with SIMPSON [29] the efficiency of a MAS $D$-HMQC experiment in between two spin-1/2 nuclei, with $D_{IS} = 1000$ Hz. Pulses other than those in recoupling sequences are ideal pulses (pulseid statement in SIMPSON). We have chosen to do the calculations for two very different spinning speeds that are both presently accessible with commercially available probes:

$\nu_R = 20$ and 70 kHz. For each recoupling sequence and each rf-field strength, the recoupling times ($\tau = NT_R$) have always been optimized. The efficiency has been normalized with respect to that obtained with a classical echo experiment ($\pi/2 - \tau - \pi - \tau$ – Acq). For the $RN_n^\nu$ sequences, we have fixed the lengths and phases of the pulses to their theoretical values (e.g. $T_R/4$, and $\pm 75°$ for $R12_3^5$) [10,14]. In SFAM sequences, we have fixed the depth of the frequency modulation $\Delta\omega_0^{max}$ to 60 kHz in $SFAM_1$ and 15 kHz in $SFAM_2$, but its optimal value span over a very broad range.

In Figs. 2 and 3, we simulated the sequence of Fig. 1a, plotting efficiencies, without any CSA (except Figs. 2b and 3b) or homo-nuclear dipolar interactions, versus the rf-field strength for $\nu_R = 20$ and 70 kHz, respectively. The maximum of efficiency is always of c.a. 70%, and only the optimum rf-field and broadness of the best matching condition is changing from method to method. One observes first that the two main $R^3$ resonances are observed at the $q = 1$ and 2 conditions (Figs. 2a and 3a), as described previously. The $q = 2$ resonance is slightly narrower than that observed for $q = 1$, which leads experimentally to a smaller efficiency when taking into account the rf-field inhomogeneity of the coil. This is one of the reason why experimentally the $q = 1$ condition should be preferred in case of weak homo-nuclear interactions. We observed that CSA of the irradiated nuclei broadens these $R^3$ resonances, as shown in Figs. 2b and 3b. However, this broadening is small, especially when $R^3$ irradiation is sent on $^1$H nuclei whose CSA is limited to c.a. 10–12 ppm. All other matching curves are much broader and should thus lead experimentally to a larger signal. $R12_3^5$ and $R20_5^9$ sequences present similar theoretical behaviors and hence should give similar experimental results (Figs. 2d and e and 3d and e). As predicted by Levitt's calculations [10,14], the main broad resonance of $R2_1^1$ (Figs. 2c and 3c) and that of $R12_3^5$ and $R20_5^9$ sequences is observed for an rf-field equal to $\nu_R$ and $2\nu_R$, respectively. This is not the case with the $SR4_1^2$ sequence for which only a large plateau is observed in between $1.5\nu_R$ and $3\nu_R$, whereas the 'analytical' optimum value corresponds to $2\nu_R$. Similar very good results are obtained with the SFAM sequences, whose efficiencies are constant over a large range (Figs. 2g and h and 3g and h). However, $SFAM_1$ requires less rf-field ($\nu_1 > \nu_R$) than $SFAM_2$ ($\nu_1 > 2\nu_R$), which thus should be mainly used in case of large homo-nuclear dipolar interactions. In the case of these very broad rf-matching curves (Figs. 2c–h and 3c-h), we have found that CSA of the recoupled nucleus has little effect on the efficiency if this CSA is smaller than the spinning speed. Up to now, we have calculated the theoretical efficiency of the $RN_n^\nu$ sequences that may be obtained with an 'ideal' probe, which means without any rise or fall time and without any phase glitches. These effects, which increase with the spinning speed, do not exist with the constant $R^3$ rf-field, and they are weak with the continuous SFAM irradiation where they mainly appear as a delay of the rf-field with respect to the amplifier voltage. To mimic these experimental limitations, we have

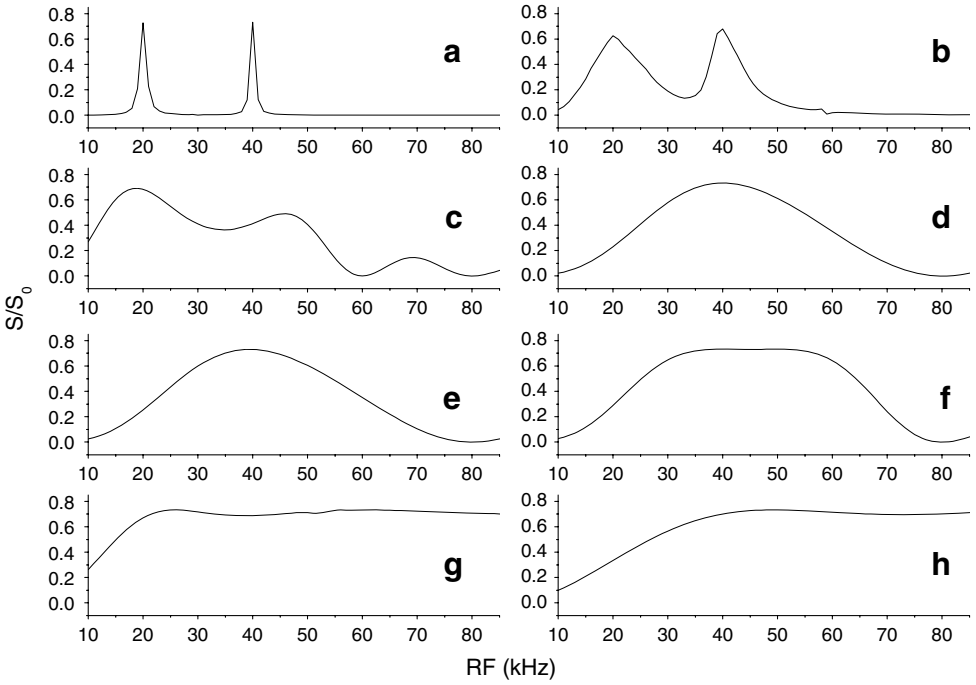


Fig. 2. Calculated optimum $^{13}$C–$^{15}$N–$^{13}$C MAS *D*-HMQC efficiency with $D_{IS} = 1$ kHz at $\nu_R = 20$ kHz, using sequence shown Fig. 1a, with ideal pulses (other than recoupling sequence), versus the rf-field amplitude ($\nu_1^{max}$ for SFAM). $R^3$ without (a) and with (b) CSA (10 kHz), $R2_1^1$ (c), $R12_3^5$ (d), $R20_5^9$ (e), $SR4_1^2$ (f), $SFAM_1$ ($\Delta\nu_0^{max} = 60$ kHz) (g), $SFAM_2$ ($\nu_0^{max} = 15$ kHz) (h). Efficiencies are normalized with respect to that observed with an echo. The same results are obtained for the simulation of $^{27}$Al–$^{31}$P–$^{27}$Al MAS *D*-HMQC using the sequence in Fig. 1a.

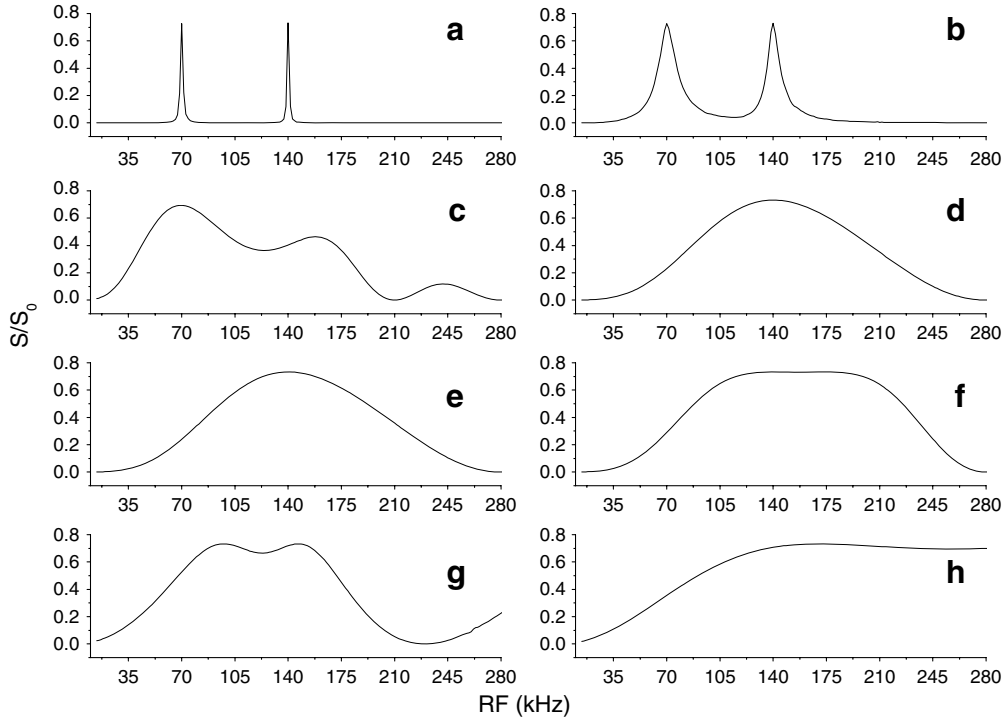


Fig. 3. Calculated optimum $^{13}C$–$^{15}N$–$^{13}C$ MAS *D*-HMQC efficiency with $D_{IS} = 1$ kHz at $\nu_R = 70$ kHz, using sequence shown Fig. 1a with ideal pulses (other than recoupling sequence), versus the rf-field amplitude ($\nu_1^{max}$ for SFAM). $R^3$ without (a) and with (b) CSA (10 kHz), $R2_1^1$ (c), $R12_3^5$ (d), $R20_5^9$ (e), $SR4_1^2$ (f), $SFAM_1$ ($\Delta\nu_0^{max} = 60$ kHz) (g), $SFAM_2$ ($\Delta\nu_0^{max} = 15$ kHz) (h). Efficiencies are normalized with respect to that observed with an echo. The same results are obtained for the simulation of $^{27}Al$–$^{31}P$–$^{27}Al$ MAS *D*-HMQC using the sequence in Fig. 1a.

redone the previous calculations, but introducing for the four previous $RN_n^\nu$ sequences a delay in between the pulses. With respect to the previous results, the efficiency of these sequences is slightly decreased and the maximum of efficiency is shifted to larger rf-fields (not shown). The scaling rf-field factor is equal to the inverse of the proportion $\varphi$ during which the rf-field is sent. As an example, the optimum rf-field is multiplied by 2.3 if the delay is of 2 μs, if $\nu_R = 70$ kHz. Obviously, the SFAM sequences still appear more appealing with respect to all other sequences when taking into account these pulse limitations. The REDOR efficiency always decreases with longer pulses (lower rf-field), and with the $XY_4$ phase cycling its value is proportional to $\cos(\pi\varphi/2)/(1\text{-}\varphi^2)$ [20].

Another important parameter is the scaling factor of the recoupled hetero-nuclear dipolar interaction which drives the optimum length for the dipolar recoupling. Remarkably its value only depends on the fact the recoupling sequence decouples or not homo-nuclear interactions:

$$SFAM_1, R^3_{q=1}, R2^1_1, \text{REDOR} \quad 2\tau_{opt} = 0.84/D \tag{3}$$

$$SFAM_2, R^3_{q=2}, SR4^2_1, R12^5_3, R20^9_5 \quad 2\tau_{opt} = 0.84\sqrt{2}/D \tag{4}$$

Previous simulations (Figs. 2 and 3) do not account for experimental signal decrease due to irreversible losses acting during the recoupling periods. These losses increase with the recoupling time. Thus, except when homo-nuclear interactions cannot be neglected, these losses are another reason to prefer sequences described in Eq. (3), and especially $SFAM_1$ and REDOR.

### 3.2. Homo-nuclear decoupling

In a second step, we have calculated the signal that can be obtained with a three spin system: two S nuclei strongly (25 kHz) dipolar coupled together, and simultaneously weakly (1 kHz) dipolar coupled with one I nucleus.

$R2_1^1$ and $SFAM_1$ do allow homo- and hetero-nuclear dipolar recoupling, hence leading to cancellation of all available magnetization. Thus they will not be considered in the following. Only one main resonance is now observed on the $R^3$ matching curves (Figs. 4a and 5a), which corresponds to the $q = 2$ condition. Again, the $R12_3^5$ and $R20_5^9$ methods behave similarly, but are much less efficient than without homo-nuclear dipolar interactions, especially at low spinning speed where this interaction is weakly MAS averaged (Figs. 4b and c and 5b and c). The $SR4_1^2$ matching curve is now split into three narrow resonances corresponding to $\nu_1/\nu_R = 2$, 3 and 5. In any case, the most efficient method is $SFAM_2$, especially when introducing the previous delay between the $RN_n^\nu$ pulses (not shown). The $SFAM_2$ matching curve is less flat than before and a broad maximum is observed for $\nu_1 = 4\nu_R$. Of course, the efficiency of all methods increases with spinning speed, as homo-nuclear interactions are then more and more averaged. The REDOR efficiency is decreased by the introduction

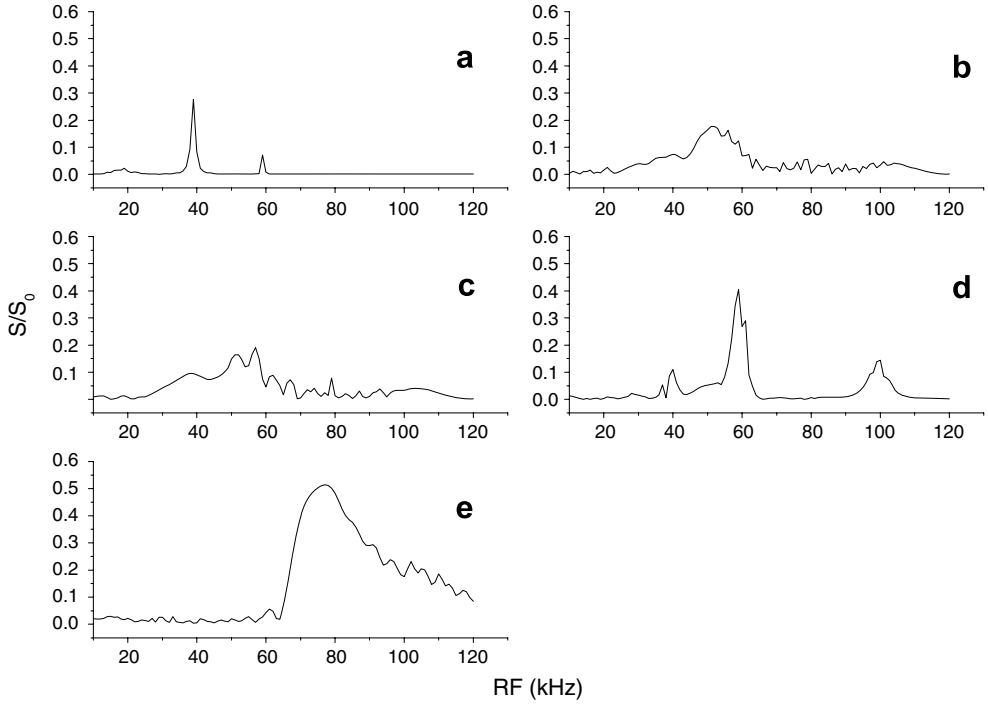


Fig. 4. Calculated optimum $^{1}H$–$^{15}N$–$^{1}H$ MAS *D*-HMQC efficiency in the case of strong homo-nuclear dipolar interaction with $D_{1H-1H} = 25$ kHz and $D_{1H-15N} = 1$ kHz, with no CSA, at $\nu_R = 20$ kHz, using sequence of Fig. 1b: with $R^3$ (a), $R12_3^5$ (b), $R20_5^9$ (c), $SR4_1^2$ (d), $SFAM_2$ ($\Delta\nu_0^{max} = 15$ kHz) (e).

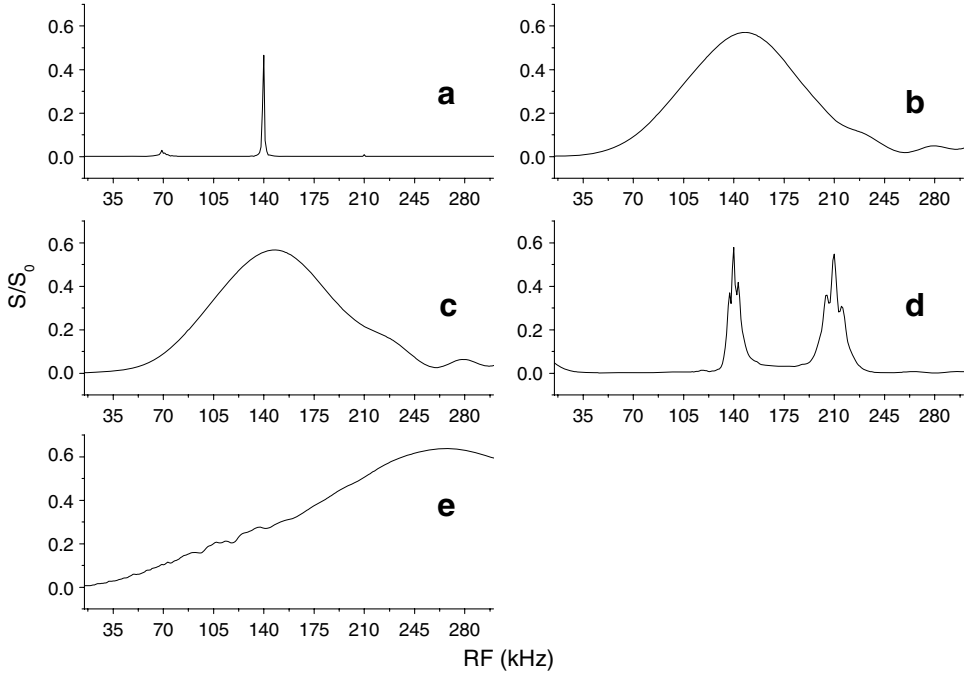


Fig. 5. Calculated optimum $^{1}H$–$^{15}N$–$^{1}H$ MAS *D*-HMQC efficiency in the case of strong homo-nuclear dipolar interaction with $D_{1H-1H} = 25$ kHz and $D_{1H-15N} = 1$ kHz, with no CSA at $\nu_R = 70$ kHz, using sequence of Fig. 1b: with $R^3$ (a), $R12_3^5$ (b), $R20_5^9$ (c), $SR4_1^2$ (d), $SFAM_2$ ($\Delta\nu_0^{max} = 15$ kHz) (e).

of the homo-nuclear interactions, especially with weak rf-fields [22].

It must be noted that in order to compare the rf-power dissipated into the coil for the various methods, the rf values indicated for SFAM are peak values (Figs. 2g and h and 3g and h) and should thus be divided by $\sqrt{2}$ to get RMS values, because they correspond to sinusoidal modulations. It is also important to note that simulations including half-integer quadrupolar nuclei (not shown), gave very similar results to those shown in Figs. 2–5.

## 4. Verifications on $^{13}C$–$^{15}N$–$^{13}C$ *D*-HMQC of glycine

We have first started to verify previous calculations in between two spin-1/2 nuclei, by recording $^{13}C$–$^{15}N$–$^{13}C$ *D*-HMQC HETCOR spectra of fully $^{13}C$ and $^{15}N$ enriched glycine at $B_o = 9.4$T and $\nu_R = 20$ kHz. There are two carbons, at 42 and 180 ppm, and a single nitrogen in this amino-acid. However, the $^{13}C$–$^{13}C$ homo-nuclear interactions are weak in glycine. In Fig. 6 is represented the optimum first slice ($t_1 = 0$) spectrum for the $^{13}C$ resonance at 42 ppm, for the various dipolar recoupling sequences. We have used a $^{1}H$ TPPM decoupling sequence during the acquisition of this first slice [30].

When the recoupling is performed indirectly on the $^{15}N$ channel all sequences perform similarly (Fig. 6), except mainly the two $R^3$ sequences, which give a very weak signal due to their narrow matching curves with respect to the coil rf-inhomogeneity. As said before, the $q = 2$ resonance efficiency is still weaker than that for $q = 1$, due to narrower resonance and longer $\tau_{opt}$ value. The $R2^1_1$ sequence is intermediate between the $R^3$ sequences and the six other sequences.

When the $^{13}C$–$^{15}N$ dipolar recoupling is performed directly on the $^{13}C$ observed channel (Fig. 7), results are completely different, as all pulses defects of the recoupling sequence (rising and falling times, phase glitches and errors, rf-field strength and spinning speed instability) are then emphasized, and prevent $^{13}C$ CSA refocusing. One striking example of this effect is the REDOR signal, which is quite decreased with respect to Fig. 6, as shown previously by Gan [8]. The normalized optimum signal intensity we achieved is: (6) REDOR, (25) $R^3_{q=2}$, (43) $R^3_{q=1}$, (47) $R2^1_1$ and $R20^9_5$, (52) $SFAM_2$, (57) $R12^5_3$, (66) $SR4^2_1$ and (80) $SFAM_1$.

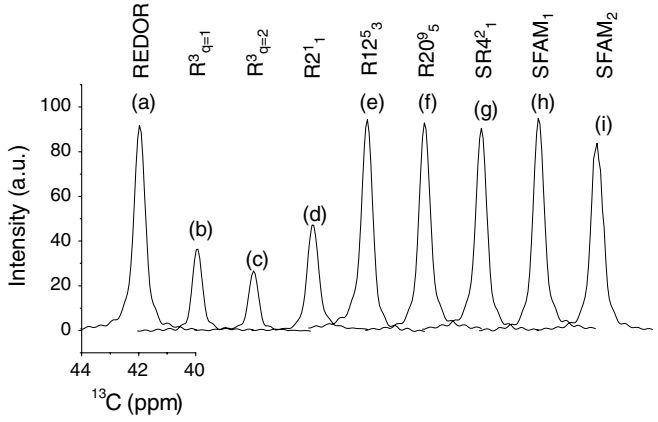


Fig. 6. Experimental $^{13}C$–$^{15}N$–$^{13}C$ MAS *D*-HMQC of glycine with recoupling sequence on the $^{15}N$ channel (sequence Fig. 1a). Only the resonance at 42 ppm is shown. $B_o = 9.4$ T, $\nu_R = 20$ kHz, $RF_C = 50$ kHz, $RF_N = 55$ kHz, number of scan is 4, recycle time is 2 s, recoupling pulse length is around 1000μs. (a) $REDOR_{XY4}$, (b) $R^3$ ($q = 1$), (c) $R^3$ ($q = 2$), (d) $R2^1_1$, (e)$R12^5_3$, (f) $R20^9_5$, (g) $SR4^2_1$, (h) $SFAM_1$ ($\nu_1^{max}$ =64 kHz, $\Delta\nu_0^{max} = 60$ kHz), (i) $SFAM_2$ ($\nu_1^{max}$ =26 kHz, $\Delta\nu_0^{max} = 15$ kHz). Intensities are normalized to the same arbitrary reference.

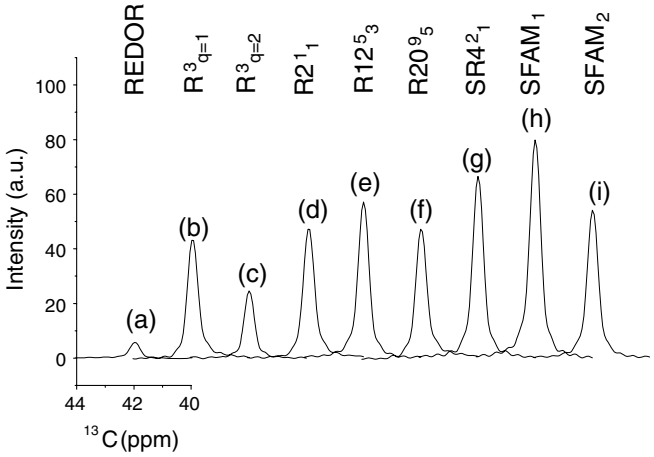


Fig. 7. Experimental $^{13}C$–$^{15}N$–$^{13}C$ MAS *D*-HMQC of glycine with recoupling sequence on the $^{13}C$ channel (sequence Fig. 1b). Only the resonance at 42 ppm is shown. $B_o = 9.4$ T, $\nu_R = 20$ kHz, $RF_C = 50$ kHz, $RF_N = 55$ kHz, number of scan is 4, recycle time is 2 s, recoupling pulse length is around 1000 μs. (a) $REDOR_{XY4}$, (b) $R^3$ ($q = 1$), (c) $R^3$ ($q = 2$), (d) $R2^1_1$, (e) $R12^5_3$, (f) $R20^9_5$, (g) $SR4^2_1$, (h) $SFAM_1$ ($\nu_1^{max} = 42$ kHz, $\Delta\nu_0^{max} = 60$ kHz), (i) $SFAM_2$ ($\nu_1^{max} = 22$ kHz, $\Delta\nu_0^{max} = 15$ kHz). Intensities are normalized to the same arbitrary reference as in Fig. 6.

## 5. Verifications on $^{27}Al$–$^{31}P$–$^{27}Al$ *D*-HMQC of $AlPO_4$ VPI5

We have performed the same type of verifications in between $^{27}Al$ and $^{31}P$ in microporous hydrated aluminophosphate $AlPO_4$-VPI5. This sample contains three equally populated sites for Al and P, which are coordinated with each other through one bridging oxygen [31]. Under MAS, the $^{31}P$ resonances are well resolved, but only two $^{27}Al$ peaks are observable. The resonance labeled $Al_1$ ($\approx -20$ ppm) represents a site between the fused four-membered rings. Two water molecules complete an octahedral coordination sphere for $Al_1$ and render inequivalent the tetrahedrally coordinated $Al_2$ and $Al_3$ sites ($\approx$ 42 ppm), as well as the phosphorus sites $P_2$ and $P_3$ in the six-membered rings. The specific connectivities between various nuclei are as follows: $Al_1$ ($2P_1$, $P_2$, $P_3$), $Al_2$ ($P_1$, $2P_2$, $P_3$) and $Al_3$ ($P_1$, $P_2$, $2P_3$). The quadrupolar coupling constants $C_Q$ for the aluminum sites are 3.95 MHz ($Al_1$), 1.3 MHz ($Al_2$), and 2.8 MHz ($Al_3$) [32]. Because we deal now with one quadrupolar nucleus with spin-5/2, the dipolar recoupling sequence must be sent onto the phosphorus channel. Due to very long phosphorus relaxation times, we have started the experiment from the aluminum channel (Fig. 1a) and thus recorded the first $t_1$ slice of $^{27}Al$–$^{31}P$–$^{27}Al$ *D*-HMQC experiments. This means that the large phosphorus CSA do not intervene in the indirect refocusing of the $^{31}P$–$^{27}Al$ dipolar coupling. The results for the $Al_{2,3}$ resonances represented in Fig. 8 are very similar to those previously obtained in case of two spin-1/2 nuclei (Fig. 6). The $R2^1_1$ and $SFAM_2$ efficiencies are intermediate between those very small observed with $R^3$ and the large ones observed for REDOR, $R12^5_3$, $R20^9_5$, $SR4^2_1$ and $SFAM_1$. Simultaneously, for three methods ($R^3_{q=1}$, $SFAM_1$,

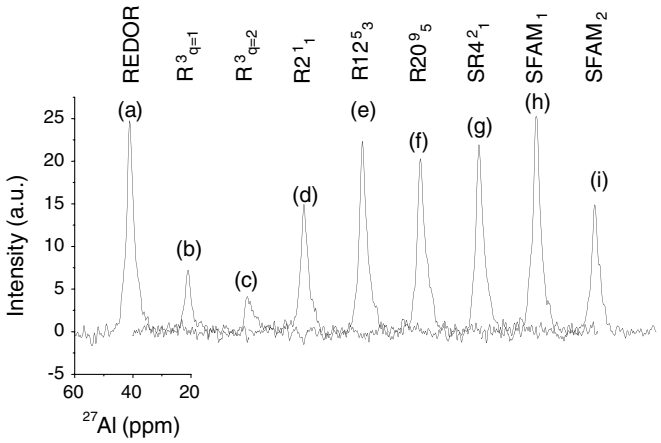


Fig. 8. Experimental $^{27}$Al–$^{31}$P–$^{27}$Al MAS *D*-HMQC of $AlPO_4$-VPI5 with recoupling sequence on the $^{31}$P channel (sequence Fig. 1a). Only the $Al_{2,3}$ resonance at 40 ppm is shown. $B_o = 9.4$ T, $\nu_R = 10$ kHz, $RF_{Al} = 7$ kHz, $RF_P = 62$ kHz, number of scan is 8, recycle time is 1 s, recoupling pulse length is around 800$\mu$s. (a) $REDOR_{XY4}$, (b) $R^3$ ($q = 1$), (c) $R^3$ ($q = 2$),$R2^1_1$ (d), $R12^5_3$ (e), $R20^9_5$ (f), $SR4^2_1$ (g), (h) $SFAM_1$ ($\nu_1^{max} = 55$ kHz, $\Delta\nu_0^{max} = 50$ kHz), (i) $SFAM_2$ ($\nu_1^{max} = 42$ kHz, $\Delta\nu_0^{max} = 50$ kHz).

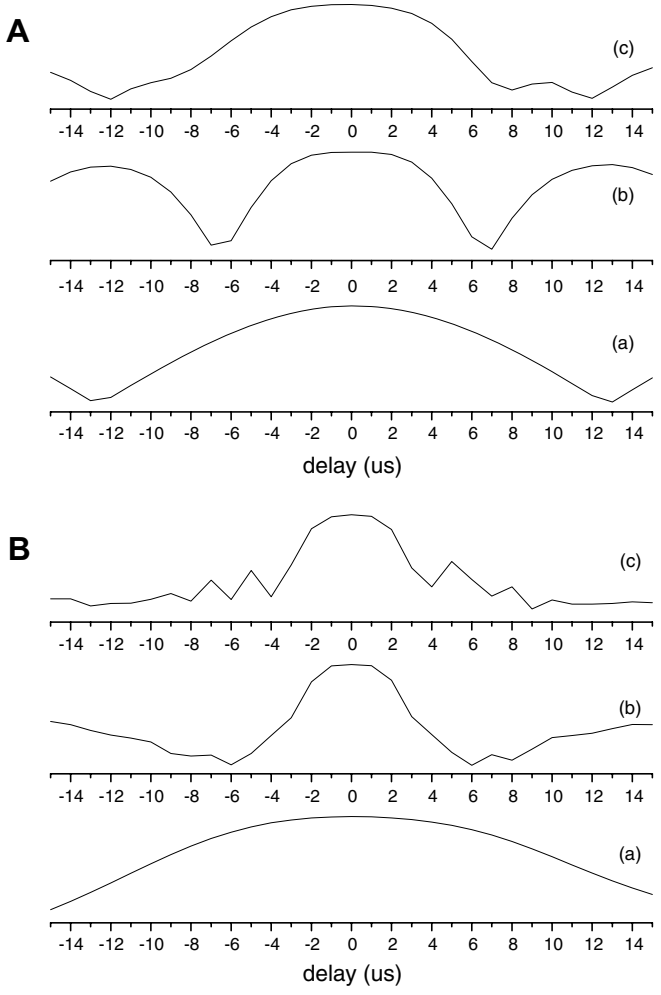


Fig. 9. Calculated synchronization effects of the delay, with respect to $kT_R$, between the two recoupling periods for the $R^3$ ($q = 1$) (a), $SR4^2_1$ (b), and $SFAM_1$ (c) ($\Delta\nu_0^{max} = 60$ kHz) sequences. $B_o = 9.4$ T, $\nu_R = 10$ kHz. The recoupling sequence is either sent on the non-observed (A) or the observed (B) channel.

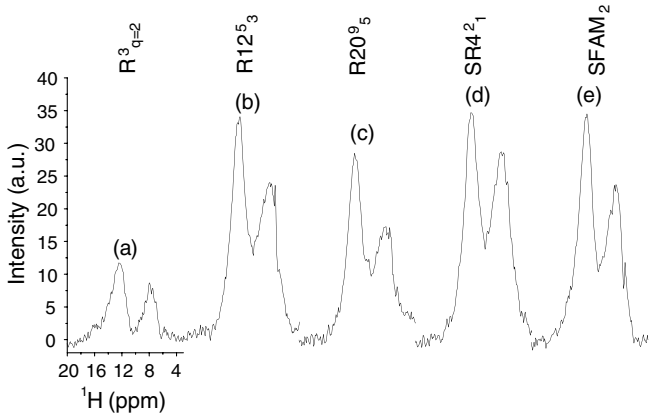


Fig. 10. Experimental $^1$H–$^{15}$N–$^1$H MAS *D*-HMQC of histidine with $B_o = 9.4$ T, $\nu_R = 20$ kHz, $RF_H = 113$ kHz, $RF_N = 65$ kHz, number of scan is 8, recycle time is 3 s, recoupling pulse length is around 200 μs. (a) $R^3$ ($q = 2$), (b) $R12^5_3$, (c) $R20^9_5$, (d) $SR4^2_1$, (e) $SFAM_2$ ($\nu_1^{max} = 71$ kHz, $\Delta\nu_0^{max} = 15$ kHz).

$SR4^2_1$), we have calculated the efficiency versus the delay (Fig. 1: $\approx kT_R$) in between the two recoupling sequences. It can be observed that the rotor-synchronization of this delay is more critical for $SR4^2_1$ than for $R^3_{q=1}$ and $SFAM_1$ (Fig. 9A). This timing is still more critical when the recoupling sequences are sent on the observed channel (Fig. 9B). Simulation results (Fig. 9) have been verified experimentally.

## 6. Verifications on $^1$H-$^{15}$N-$^1$H *D*-HMQC of histidine

There are three different types of protons in histidine, but only two resonances are observed at 8 and 12 ppm, with the spinning speed ($\nu_R = 20$ kHz) and static field ($B_o = 9.4$ T) we have used. In this case, it is mandatory using a recoupling sequence that also decouples the $^1$H-$^1$H dipolar interactions, and therefore the signal observed with REDOR, $R^3_{q=1}$, and $SFAM_1$ sequences was always very small (not shown). In Fig. 10, we have thus only represented the first slice observed with the five sequences ($R^3_{q=2}, SR4^2_1, R12^5_3, R20^9_5, SFAM_2$) described in Eq. (4) with the recoupling sequence sent on the $^{15}$N channel. The optimum recoupling periods for these sequences were always similar and approximately 1.4 longer than that observed with REDOR, $R^3_{q=1}$, and $SFAM_1$. Except for the $R^3_{q=2}$ recoupling scheme, which behaves poorly due to the narrowness of its resonance, the four other sequences present approximately the same efficiency at this spinning speed. However, we believe that, in opposite to $SFAM_2$, the efficiency of $RN^v_n$ recoupling sequences will largely decrease at very fast spinning speed, due to pulse imperfections.

## 7. Conclusions

We have compared several hetero-nuclear dipolar recoupling sequences to be used with indirectly detected MAS *D*-

H-M/S-QC experiments in between a spin-1/2 and a quadrupolar nucleus. In any cases, it must be noted that $R^3$ methods behave very poorly due to the narrowness of their rf-matching curves.

When homo-nuclear interactions are negligible, and when the recoupling sequence is sent on the non-observed channel, most of the sequences present approximately the same efficiency. However, three sequences should be preferred because of their shorter minimum length, REDOR, $SFAM_1$ (one rotor-period) and $SR4_1^2$ (two rotor-periods), which allows for a better optimization of the contact times. Indirect $SFAM_1$ is very robust, as rotor synchronization of the delay between the two recoupling periods is not critical, and also because its associated losses are smaller than with $SR4_1^2$, due to a shorter contact time. When the recoupling sequence is sent on the observed channel, only two methods emerge: $SR4_1^2$ and especially $SFAM_1$. The advantage of the method $SR4_1^2$, is that it can be done with old consoles, as it requires only pulses with phases $\pm 90°$. However, $SFAM_1$ is still more efficient, especially at very high spinning speed.

When homo-nuclear interactions are not negligible, the most interesting recoupling sequences are $R12_3^5, R20_5^9, SR4_1^2$ and $SFAM_2$. However, the experimental comparisons have been performed at $\nu_R = 20$ kHz, and it is predictable that the advantage of $SFAM_2$ with respect to all other sequences will increase with the spinning speed. Indeed, $SFAM_2$ uses continuous modulations of frequency and amplitude, and is thus very little subject to classical pulse-limitations (rise and fall times, phase glitches), which is not the case with the $RN_n^\nu$ recoupling sequences.

We have always observed similar optimum recoupling periods for all methods that decouple homo-nuclear dipolar interactions ($R_{q=2}^3, SR4_1^2, R12_3^5, R20_5^9, SFAM_2$), and this optimum length was approximately 1.4 longer than that observed with sequences that do not decouple these interactions ($R_{q=1}^3$, REDOR, $SFAM_1$). This is one of the reasons why $SFAM_1$ should be preferred in case of weak homo-nuclear dipolar interactions, especially at very fast spinning speeds.

The robustness of $RN_n^\nu$ sequences with respect to chemical shielding, rf-inhomogenity, and instrumental errors in phase setting can be improved by supercycling [33–35]. However, we anticipate that SFAM methods, which are very simple and robust, will become very fast the methods of choice, especially at very fast MAS. Moreover, the robustness of the SFAM methods may still be increased also by supercycling.

## Acknowledgments

Authors thank Region Nord/Pas de Calais, Europe (FEDER), CNRS, French Minister of Science, USTL, ENSCL, FR-3950 and the Bruker company for funding. They also thank Drs. S. Antonijevic and A. Brinkmann for the numerous fruitful discussions. At Lille, this research was supported by the ANR contract NT05-2-41632.

## References

[1] L. Müller, Sensitivity enhanced detection of weak nuclei using heteronuclear multiple quantum coherence, J. Am. Chem. Soc. 101 (1979) 448–4484.

[2] G. Bodenhausen, D.J. Ruben, Natural abundance nitrogen-15 NMR by enhanced heteronuclear spectroscopy, Chem. Phys. Lett. 69 (1980) 185–189;
A.A. Maudsley, R.R. Ernst, Indirect detection of magnetic resonance by heteronuclear two-dimensional spectroscopy, Chem. Phys. Lett. 50 (1977) 368–372.

[3] E.R. Andrew, A. Bradbury, R.G. Eades, Nuclear magnetic resonance spectra from a crystal rotated at high speed, Nature 182 (1958) 1659.

[4] S.R. Hartmann, E.L. Hahn, Nuclear double resonance in the rotating frame, Phys. Rev. 128 (1962) 2042–2053.

[5] A. Pines, M.G. Gibby, J.S. Waugh, Proton-enhanced NMR of dilute spins in solids, J. Chem. Phys. 59 (1973) 569–590.

[6] A. Lesage, D. Sakellariou, S. Steuernagel, L. Emsley, Carbon–proton chemical shift correlation in solid-state NMR by through-bond multiple-quantum spectroscopy, J. Am. Chem. Soc. 120 (1998) 13194–13201;
D. Massiot, F. Fayon, B. Alonso, J. Trébosc, J.P. Amoureux, Chemical bonding differences evidenced from *J*-coupling in solid-state NMR experiments involving quadrupolar nuclei, J. Magn. Reson. 164 (2003) 160–164;
J.P. Amoureux, J. Trébosc, J. Wiench, M. Pruski, HMQC and refocused-INEPT experiments involving half-integer quadrupolar nuclei, J. Magn. Reson. 184 (2006) 1–14.

[7] A. Lesage, L. Emsley, Through-bond heteronuclear single-quantum correlation spectroscopy in solid-state NMR, and comparison to other through-bond and through-space experiments, J. Magn. Reson. 148 (2001) 449–454.

[8] Z. Gan, $^{13}C/^{14}N$ heteronuclear multiple-quantum correlation with rotary resonance and REDOR dipolar recoupling, J. Magn. Reson. 184 (2006) 39–43;
J. Trébosc, B. Hu, J.P. Amoureux, Z. Gan, Through-space $R^3$ HETCOR experiments between spin-1/2 and half-integer quadrupolar nuclei in solid-state NMR, J. Magn. Reson. 186 (2007) 220–227.

[9] M.H. Levitt, T.G. Oas, R.G. Griffin, Rotary resonance recoupling in heteronuclear spin pair systems, Israel J. Chem. 28 (1988) 271;
T.G. Oas, R.G. Griffin, M.H. Levitt, Rotary resonance recoupling of dipolar interactions in solid-state nuclear magnetic resonance spectroscopy, J. Chem. Phys. 89 (1988) 692–695;
Z. Gan, D.M. Grant, Rotational resonance in a spin-lock field for solid state NMR, Chem. Phys. Lett. 168 (1990) 304–308;
Z. Gan, D.M. Grant, R.R. Ernst, NMR chemical shift anisotropy measurements by RF driven rotary resonance, Chem. Phys. Lett. 254 (1996) 349–357.

[10] A. Brinkmann, M.H. Levitt, Symmetry principles in the nuclear magnetic resonance of spinning solids: Heteronuclear recoupling by generalized Hartmann–Hahn sequences, J. Chem. Phys. 115 (2001) 357–384.

[11] A. Brinkmann, A.P.M. Kentgens, Sensitivity enhancement and heteronuclear distance measurements in biological $^{17}O$ solid-state NMR, J. Phys. Chem. B 110 (2006) 16089–16101.

[12] A. Brinkmann, A.P.M. Kentgens, Proton-selective $^{17}O$-$^{1}H$ distance measurements in fast MAS solid-state NMR spectroscopy for the determination of hydrogen bond lengths, J. Am. Chem. Soc. 128 (2006) 14758–14759.

[13] S. Cavadini, A. Abraham, G. Bodenhausen, Proton-detected $^{14}N$ NMR by recoupling of heteronuclear dipolar interactions using symmetry-based sequences, Chem. Phys. Lett. 445 (2007) 1–5.

[14] M. Carravetta, M. Eden, X. Zhao, A. Brinkmann, M.H. Levitt, Symmetry principles for the design of radiofrequency pulse sequences in the nuclear magnetic resonance of rotating solids, Chem. Phys. Lett. 321 (2000) 205–215;

X. Zhao, M. Eden, M.H. Levitt, Recoupling of heteronuclear dipolar interactions in solid-state NMR using symmetry-based pulse sequences, Chem. Phys. Lett. 342 (2001) 353–361;
M.H. Levitt, Symmetry-based pulse sequences in MAS solid-state NMR, in: D.M. Grant, R.K. Harris (Eds.), Encyclopedia of NMR, vol. 9, Wiley, Chichester, England, 2002.

[15] T. Gullion, J. Schaefer, Rotational-echo double resonance NMR, J. Magn. Reson. 81 (1989) 196–200.

[16] R. Fu, S.A. Smith, G. Bodenhausen, Recoupling of heteronuclear dipolar interactions in solid-state MAS NMR by simultaneous frequency and amplitude modulation, Chem. Phys. Lett. 272 (1997) 361–369;
K. Nishimura, R. Fu, T.A. Cross, The effect of RF-inhomogeneity on heteronuclear dipolar recoupling in solid-state NMR: practical performance of SFAM and REDOR, J. Magn. Reson. 152 (2001) 227–233.

[17] Z. Gan, J.P. Amoureux, J. Trébosc, Proton-detected $^{14}$N MAS NMR using homonuclear decoupled rotary resonance, Chem. Phys. Lett. 435 (2007) 163–169.

[18] T. Gullion, D.B. Baker, M.S. Conradi, New compensated Carr-Purcell sequences, J. Magn. Reson. 89 (1990) 479–484;
T. Gullion, J. Schaefer, Elimination of resonance offset effects in rotational-echo double-resonance NMR, J. Magn. Reson. 92 (1991) 439–442.

[19] L. Chopin, R. Rosanske, T. Gullion, Simple improvements in spinning-speed control for MAS experiments, J. Magn. Reson. A122 (1996) 237–239;
T. Gullion, A.J. Vega, Measuring heteronuclear dipolar couplings for $I = 1/2$, $S > 1/2$ spin pairs by REDOR and REAPDOR NMR, Prog. Nucl. Mag. Res. Spec. 47 (2005) 123–136.

[20] C.P. Jaroniec, B.A. Tounge, C.M. Rienstra, J. Herzfeld, R.G. Griffin, Recoupling of heteronuclear dipolar interactions with REDOR at high-MAS frequencies, J. Magn. Reson. 146 (2000) 132–139.

[21] M. Baldus, B.H. Meier, Broadband polarization transfer under magic-angle spinning: application to total through-space-correlation NMR spectroscopy, J. Magn. Reson. 128 (1997) 172–193.

[22] R. Tycko, G. Dabbagh, Measurement of nuclear magnetic dipole–dipole couplings in magic angle spinning NMR, Chem. Phys. Lett. 173 (1990) 461–465.

[23] N.C. Nielsen, H. Bildsoe, H.J. Jakobsen, Double-quantum homonuclear rotary resonance: efficient dipolar recovery in magic-angle spinning nuclear magnetic resonance, J. Chem. Phys. 101 (1994) 1805–1812;
R. Verel, M. Baldus, M. Ernst, A homonuclear spin-pair filter for solid-state NMR based on adiabatic-passage techniques, Chem. Phys. Lett. 287 (1998) 421–428.

[24] N.C. Nielsen, H. Bildsoe, H.J. Jakobsen, M.H. Levitt, Double-quantum homonuclear rotary resonance: efficient dipolar recovery in magic-angle spinning nuclear magnetic resonance, J. Chem. Phys. 101 (1994) 1805–1812;
Y.K. Lee, N.D. Kurur, M. Helmle, O.G. Johannessen, N.C. Nielsen, M.H. Levitt, Efficient dipolar recoupling in the NMR of rotating solids. A sevenfold symmetric radiofrequency pulse sequence, Chem. Phys. Lett. 242 (1995) 304–309.

[25] A. Brinkmann, J. Schmedt auf der Günne, M.H. Levitt, Homonuclear zero-quantum recoupling in fast magic-angle spinning nuclear magnetic resonance, J. Magn. Reson. 156 (2002) 79–96;
T. Karlsson, J.M. Popham, J.R. Long, N. Oyler, G.P. Drobny, A study of homonuclear dipolar recoupling pulse sequences in solid-state nuclear magnetic resonance, J. Am. Chem. Soc. 125 (2003) 7394–7407;
P.E. Kristiansen, M. Carravetta, W.C. Lai, M.H. Levitt, A robust pulse sequence for the determination of small homonuclear dipolar couplings in magic-angle spinning NMR, Chem. Phys. Lett. 390 (2004) 1–7.

[26] P.K. Madhu, X. Zhao, M.H. Levitt, High-resolution $^{1}$H NMR in the solid-state using symmetry-based pulse sequences, Chem. Phys. Lett. 346 (2001) 142–148.

[27] P.K. Madhu, A. Goldbourt, L. Frydman, S. Vega, Sensitivity enhancement of the MQMAS NMR experiments by fast amplitude modulation of the pulses, Chem. Phys. Lett. 307 (1999) 41–47;
P.K. Madhu, A. Goldbourt, L. Frydman, S. Vega, Fast radio-frequency amplitude modulation in multiple-quantum magic-angle spinning nuclear magnetic resonance: theory and experiments, J. Chem. Phys. 112 (2000) 2377–2391.

[28] E. van Veenendaal, B.H. Meier, A.P.M. Kentgens, Frequency steeped adiabatic passage excitation of half-integer quadrupolar spin system, Mol. Phys. 93 (1998) 195–213;
A.P.M. Kentgens, R. Verhagen, Advantages of double-frequency sweep in static, MAS, and MQMAS NMR of spin $I = 3/2$ nuclei, Chem. Phys. Lett. 300 (1999) 435–443.

[29] M. Bak, N.C. Nielsen, SIMPSON: a general simulation program for solid-state NMR pectroscopy, J. Magn. Reson. 147 (2000) 296–330.

[30] A.E. Bennet, C.M. Rienstra, M. Auger, K.V. Lakshmi, R.G. Griffin, Hetero-nuclear decoupling in rotating solids, J. Chem. Phys. 103 (1995) 6951–6958.

[31] L. B McCusker, Ch. Baerlocher, E. Jahn, M. Bülow, The triple helix inside the large-pore aluminophosphate molecular sieve VPI-5, Zeolites 11 (1991) 308–313.

[32] J. Rocha, W. Kolodziejski, H. He, J. Klinowski, Solid-state NMR studies of hydrated porous aluminophosphate VPI-5, J. Am. Chem. Soc. 114 (1992) 4884–4888;
C. Fernandez, C.M. Morais, J. Rocha, M. Pruski, High-resolution hetero-nuclear correlation spectra between $^{31}$P and $^{27}$Al in Microporous Aluminophosphates, Solid State Nucl. Magn. Reson. 21 (2002) 61–70.

[33] M. Carravetta, M. Eden, O.G. Johannessen, H. Luthman, P.J.E. Verdegem, J. Sebald, A. Sebald, M.H. Levitt, Estimation of carbon–carbon bond lengths and medium-range internuclear distances by solid-state nuclear magnetic resonance, J. Am. Chem. Soc. 123 (2001) 10628–10638.

[34] A. Brinkmann, J. Schmedt auf der Günne, M.H. Levitt, Homonuclear zero-quantum recoupling in fast magic-angle spinning nuclear magnetic resonance, J. Magn. Reson. 156 (2002) 79–96.

[35] M. Eden, Order-selective multiple-quantum excitation in magic-angle spinning NMR: creating triple-quantum coherences with a trilinear hamiltonian, Chem. Phys. Lett. 366 (2002) 469–476.